1.1 Literature survey

Most of chemical researches begin with answering questions related to molecular structure owing to the great connection between structure with properties and functions. This becomes particularly exciting when new molecules with novel structures are synthesized or identified if there is the prospect for novel physical or chemical properties, as might be suggested from known correlations.

Although the determination of molecular structure has long essentially been depending upon spectroscopic, tools, however, another set of tools has emerged in the last few decades.

It is the direct application of rigorous quantum mechanical principles by way of large scale computations or the application of calculational methods devised from fundamental chemical and physical concepts.

There are some of the abstracts that are related to the topics treated in this thesis:

G. H. Rosenblatt,etal [1] reported time-resolved spectra of luminescence from F and F^+ centers in MgO excited at 248 nm over 8 decades of time and intensity, from 20 ns to 2s. The decay time of F and F^+ luminescence had been measured at temperatures ranging from 90 to 573K. The luminescence yield and spectra were studied as a function of excitation-power density at 248 nm over a span of 10 decades, from 1 mW/cm^2 to 38 MW/cm^2. Higher pump-power density favors F luminescence over F^+ luminescence in thermochemically reduced crystals, and the luminescence yield saturated above about 50 KW/cm^2 of pump intensity.

Transient absorption spectra were measured in the microsecond-to-seconds time range. The luminescence data showed that the decay kinetics of excited F and F^+ centers were dominated by ionization from the excited state and charge recapture from traps which included the H^- center in thermochemically reduced MgO. It is furthermore inferred that electrons are the charge carried having primary influence on kinetics of both F and F^+ centers. This implied that the F^+ first-excited state lied close to the conduction-band edge. We confirmd that excitation at 48nm also caused released of valence holes, and propose a mechanism which may explained the hole released, the increased of the F-to-F^+ intensity ratio with increased pump intensity, and the saturation of luminescence with increased pump intensity.

G. P. Summers, etal [2] reported experimental measurements and theoretical calculations that may resolve some of remaining difficulties associated with photoemission from anion vacancies in thermochemically reduced MgO crystals. The intensities of the 2.3- and 3.2- eV luminescence bands were fond to be strongly influenced by both the concentrations of H^- ions and anion vacancies present, and also by the intensity of the ~5.0-eV exciting light.

Theoretical calculations predicted that for a $^1A_{1g}$ relaxation of surrounding ions the $^1T_{1u}$ and $^3T_{2u}$ electronic states of the F center were almost degenrated and ~0.05eV above the $^3A_{1g}$ state. The $^1T_{1u} \rightarrow {}^1A_{1g}$ and the $^3T_{1u} \rightarrow {}^1A_{1g}$ transition energies are predicted to be 2.2 and 2.9eV, respectively.

Z. C. Guo and L. W. Bruch,[3] evaluated the electrostatic polarization energy for atomic hydrogen and helium in the very

nonuniform fields near the LiF(001) and MgO(001) surfaces. The variational trial functions, which for helium were at the Hartree-Fock level, included configurations corresponding to many orders of multipole polarizability. The results for helium followed the trends expected linear nonuniform response theory. The multipole series of second order perturbation theory for the polarization energy diverges for atomic hydrogen on these substrates; the calculations showd comparable contributions from the first four multipole terms. The point-ion-substrate model had a charge-transfer pathology for H MgO(001). The effective polarizability of the adatoms were calculated and the electrostatic contribution to the corrugation energy amplitude were estimated. Consequences for more polarizable inert gases were discussed.

V. Musolion, etal [4] reported density functional calculations of the stractural and dynamical properties of small copper clusters (Cu_n. n=2.5) adsorbed on the MgO (100). As Cu-Cu intracluster Interactions were stronger than cluster-surface, the most stable geometries were found to be similar to those in the gas phase, with the cluster in an upright position with respect to the surface. Further *ab initio* molecular dynamics simulations indicated that the adsorbed clusters diffuse by "rolling" and "twisting" motion, with barriers that might be smaller than that for the hopping diffusion of a single adatom.

Yu. F. Zhukovski, etal [5] carried out ab initio calculations and showed that surface defects caused redistribution of the electron density which could increase substantially the binding energy of metal atoms to oxide surfaces. The results for electron (E,") and hole (V,") centers in the adhesion of Ag atoms (at 1:4 and 1:1 coverages) to a MgO(200) surface,

combined with previous studied for charged defects, supported earlier ideas of the mechanism of radiation enhanced adhesion of non reactive metals on oxide substrates. The results suggested that some optical control of adhesion energies was possible through charge transfer.

Z. F. Liu, etal [6] used *ab initio* molecular dynamics (MD) method, based on density functional theory (DFT) with plane waves and pseudopotentials, to studied the stability and internal motion in silver cluster Ag_n. with n=4-6. Calculations on the neutral, cationic and anionic silver dimer Ag_2 showed that the bond distance and vibrational frequency calculated by DFT were of good quality. Simulations of Ag_4, Ag_5, and Ag_6 in canonical ensemble reveal distinct characteristics and isomerization paths for each cluster. At a temperature of 800K, an Ag_4 had no definite structure due to internal motion,while for Ag_5 and Ag_6 the clusters maintained the planar structure, with atomic rearrangement observed for Ag_5 but not for Ag_6. At a temperature of 200K, Ag_4 could exsit in two planar structures whilst Ag_5 was found to be stable only in the planar form. In contrast Ag_6 was stable in both planar triagonal and 3D pentagonal structures. Micro-canonical MD simulation was performed for all three clusters to obtain the vibrational density of states.

J. B. Forcsman, etal [7] used reviewed the methodological and computational considerations necessary for the determination of the *ab initio* energy, wave function, and gradient of a molecule in an electronically excited state using molecular orbital theory. In particular, the authors reexamined a fundamental level of theory which was employed several years ago for the interpretation of the electronic spectra

of simple organic molecules, configuration interaction (CI) among all singly substitued determinants using a Hartree-Fock reference state. This investigation presented several new enhancements to this general theory. First, it was shown how the 'CI-singles' wave function could be used to compute efficiently the analytic first derivative of the energy in order to obtain accurate properties and optimized geometries for a wide range of molecules in their excited states. Second a computer program was described which allowed these computations to be did in 'direct' fashion, with no disk storage required for the tow-electron repulsion integrals.

P. W. M. Jacobs,[8] reviewed the methods avilable for the calculation of defect Gibbs energies by computer calculations. The applicability of the ionic model to AgCl and AgBr was discussed: the proximity of the filled 4d level and vacant 5s level in Ag^+ made possible d $\longrightarrow$ s excitations that induced a quadrupolar deformation of the Ag^+ ion;these excitations also promte a Jahn-Teller disortion of the $Ag^+X^-_6$ molecule and probably other deformations as well, and they might lead to partial covalence. Methods of arriving at Van der Waals coefficients for AgX were described and various ways of improving previously used two-body potentials were discussed. The possibility of evaluating surface potentials theoretically was considered.

K. B. Shelimov, etal [9] reported *ab initio* calculations of the geometry, electronic structure, ionization and excitation energies of an M-center on the AgBr (100) surface. This structure, formed in the process of surface reduction, might be viewed as an Ag_2 molecule adsorbed on the AgBr (100) surface with a 'pit' and might be become a primary center for photographic formation. The authors found the equilibrium position of

the Ag_2 molecule 0.62Å above the surface and the adsorption energy 0.88eV. The Σ_g Σ_u excitation energies were greater by 0.6-1.0 eV and ionization potentials were 1.3-1.8 eV less than those for the free molecule. The results of the calculations which did and did not treat Ag 4d electrons explicitly match each other well. The adsorpation energy was compared with that in other *ab initio* Ag_n/ AgBr (100) calculations.

O. B. Piven and A. M. Gusak,[10] suggested a numerical model which described growth of silver particles in the surface layer of AgBr microcrystals under laser irradiation. Processes of recombination of electrons, holes, silver ions Ag^+ and the decrease of the volume of silver particles due to diffusion of Ag^+-ions and neutral Ag^0-atoms (in time intervals, when particles remain neutral) were taken into account simultaneously. Model calculations of Ag particle sizes coincide with reasonable accuracy with experimental data.

M. T. Olm and R. S. Eachus, [11] the high imaging efficiency of today's color negative film depended on the unique defect properties of silver halides. We had chosen two important defect topics to high light; defect- induced anisotropic crystal growth, and shallow electron trapping at surface defects and transition metal dopant sites. High imaging efficiency was depend on the ability to concentrate photoelectrons and there by to form a single latent image center per crystalline. This required electron localization at a partially-charged, shallow electron trap at the surface followed by a shallow-deep transition to a metastable atom state. Subsequent ionic and electronic trapping processes that built the latent image occur only at this site. In some cases, doping the bulk of the microcrystal intrinsic shallow electron traps could improve latent image

formation efficiency. Electron concentration did not occur at these dopant sites since they were not partially charged. Magnetic resonance and photoconductivity studied of the dynamics of shallow trapping by dopants and of the shallow–deep transition at surface sites were presented.

A. S. Shalabi, etal [12] an attempt had been made to compare between the energetic properties of the self trapped hole STH center in LiF and NaH isoelectronic crystals, using an embedded cluster model and second order Moller-Plessent perturbation correction of *ab initio* theory. LiF and NaH clusters were embedded in simulated Coulomb fields that closely approximate the Madlung potentials of the host crystal and STH reorientation, band structure and adsorptivity of atomic *H* were examined. LiF and NaH clusters in crystals were found to exhibit differences in the energetic properties. While the off-center configuration in the bulk of LiF was more stable than the on-center configuration, the on-center configuration in the bulk of NaH was more stable. The activation energy barriers were calculated to be 0.07 and 0.30 eV for bulk and surface diffusion of STH in LiF, and 0.66 and 0.60 eV for bulk and surface diffusion of STH in NaH. On basis of X2- bond elongation, LiF surface crystalline potentials were found to be less important than those of NaH. The order of stability of atomic *H* over LiF and NaH surfaces was totally reversed under the effect of STH imperfection. The STH enhanced the adsorptivity of atomic *H* by ca. 4.49 and 3.85 eV on LiF and NaH surfaces respectively, and changed the nature of adsorption from physical adsorption to chemical adsorption. The dramatic increase in adsorption energies was found to be attributed to spin pairing rather than the differences in energy gaps between adsorbate and substrate electrons in the course of adsorbate substrate interactions.

A. S. Shalabi, etal [13] investigated F^+ laser performance and interaction of the title group IB transition metals at the reduced oxygen coordination of MgO surface using the TD and DFT methods of *ab initio* molecular electronic structure calculations. The considered ion clusters were embedded in simulated Coulomb fields that closely approximate the Madelung fields of the host surfaces and the nearest neigbor ions to the F^+ site were allowed to relax to equilibrium in each case. The F^+ laser performance fades quickly as the reduced oxygen coordination decreases from 5 to 4 to 3. The relaxed excited states RES of the defect containing surfaces are compact and deep below the conduction bands of the perfect MgO surface. The probability of orientational destruction of the center in laser experiment was excepected to follow the order: flat>corner>edge. The excited state at the edge has higher energy than that at the flat or at the corner. F^+ was easily formed at the lower oxygen coordination and the disappearance of anisotropy and 2p splitting observed in absorption of F^+ at the surface followed the order corner>flat>edge. The Glanser-Tompkins relation was generalized to include the F^+ bands at the reduced oxygen coordination of a metal oxide surface. As far as the adsorbate-substrate interactions were concerned, the F^+ center enhanced the adsorptivity of Ag, Cu and Au by ca. 1.91-3.33 eV and changed the nature of adsorption from physical adsorption to chemical adsorption. The order of adsorption energies followed the order Cu>Au>Ag and was explainable in terms of electrostatic potential curves, energy gaps and spin pairing. Cu and Ag acted as electron donors while Au acted as electron acceptor and the MgO surface could not be made semiconducting by F^+ imperfection.

Chengteh Lee, etal [14] expressed the correlation energy density in terms of the electron density and Laplacian of the second-order Hartree-Fock density matrix, was restated as a formula involving the density and local kinetic-energy density. On insertion of gradient expansions for the local kinetic-energy density, density-functional formulas for the correlation energy and correlation potential were then obtained. Through numerical calculations on a number of atoms, positive ions, and molecules, of both open- and closed-shell type, it was demonstrated that these formulas, like the original Colle-Salvetti formulas, gave correlation energies with in a few percent.

M. M. Kuklja, etal [15] calculated the atomic and electronic structure of H^- ions substituting for O^{-2} ions in regular sites in MgO crystals using an *ab initio* Hartree-Fock (HF) cluster approached and its semiempirical version, intermediate neglect of the differential overlap. The theoretical optical absorption energy was predicted to be 10 eV, which was supported by analysis of experimental data for the H^- centers in a series of ionic crystals. The HF simulation of H^- ion diffusion via direct interstitial hops along the [100] axis predicted an activation energy of about 3 eV.

E. Heifets, etal [16] calculated the atomic and electronic structure of the Ag/MgO(100) interface by means of the *ab initio* Hartree-Fock approach combined with asupercell model. The electronic density distribution and the interface binding energy /distance were analyzed for different Ag adsorption positions, slabs of different thicknesses and varying Ag surface coverage. It was demonstrated that the adhesion

energy arises mainly due to the electrostatic interaction of substrate atoms with a complicated charge redistribution in the metal layer(s), characterized by large quadrupole moments as well as electron density redistribution towards-bridge and hollow positions between the nearest and next-nearest Ag atoms.

G. Pacchioni and P. Pescarmona, [17] performed ab initio Hartree-Fock cluster model calculations on the electronic structure and properties of neutral and charged oxygen vacancies, the F color centers, at various sites of the MgO(001) surface. Sub-surface, surface, step, and corner sites have been considered. For each site we had determined the optimal structure, the relative stability of neutral versus charged vacancies, the formation energy, and for the paramagnetic F^+ centers, the spin distribution as given by the isotropic hyperfine coupling constants of the diffusion of oxygen ions in the presence of F^{2+} centers had been estimated for the migration from the sub-surface to the surface, from a terrace site to another terrace site, and from a step to a terrace site.

J. Goniakowski, [18] presented an *ab initio* full-potenial linear muffin-tin orbital studied of the electronic structure of a palladium deposit on the MgO(100) surface. By considering three model expitaxial deposits-a bilayer, a monolayer, and one-fourth of a monolayer-we had accessed the characteristics of the evolution of the interfacial bonding as a function of the amount of the deposited metal. We found that the adsorpation was the strongest for isolated palladium atoms, and that its strength decreases with growing metal coverage. We related this

calculated tendency to change of the chemical bonding between the deposited palladium and the surface anions.

P. Cortona and A. V. Monteleone, [19] performed *ab initio* self-consistent calculations of the standard cohesive properties (equiliprium lattice parameters, binding energies and bulk moduli) of the four alkali-earth oxides (MgO, CaO, SrO and BaO) having the B1 (NaCl-like) phase under normal temperature and pressure conditions. We had also studied the relative stability of the B1 and B2 (CsCl-like) phases, and the behaviour, under pressure of these crystals (equations of state, transition pressures and changed of volume for the structural phase transition B1-B2). All the calculations were performed in the framework of the density-functional theory by a method which allowed the direct calculation of the ground-state electron density of a system without the preliminary determination of its wave functions and energy eigen values.

A. M. Ferrari and G. Pacchioni, [20] studied the interaction of O_2 and CO gas-phase molecules with oxygen vacancies on the MgO(100) surface by means of cluster models and *ab initio* wave functions. It was found that the surface oxygen vacancies, or F centres, exhibit a high reactivity toward O_2 and CO at variance with the regular MgO surface. The reaction proceeded through the formation of radical anions, O_2^- and CO^-, via the transfer of one electron trapped in the surface cavity to the empty levels of the adsorbed molecule. The resulting surface complexes, X^-/F^+ or $X^-/F2^+$ ($X=O_2$or CO), were found by electrostatic forces. Although the mechanism of the interaction was the same for the tow molecules, the details of the energetics were different, O_2 spontaneously

removed the electrons trapped in the MgO oxygen vacancies to form the stable O_2^- superoxide anion. On the contrary, CO^- forms only at finite temperatures and was a metastable species. The different behaviour could be rationalized in terms of electron affinities of the tow molecules. The calculations were useful also for the spectrorscopic characterization of the radical anions at the surface. The calculations of electron paramagnetic resonance (EPR) hyperfine coupling constants and, for CO, of the vibrational frequancies indicated that the experimental spectra were consistent with the existence of O_2^- and CO^- surface species. The analysis of the vibrational shifts showed that the coordination mode of CO is C-down and not O-down.

1.2.Computational Techniques:

1.2.1. Crystal simulation

There are several methods to simulate crystals, either by finite or infinite systems. In the case of finite systems, only local portions of the crystal are considered. For such an approach, clusters of varying sizes in bulk structure are suitable approximations. Here one must distinguish between free clusters, saturated clusters and embedded clusters. Free clusters are simply parts of the bulk, and their simulations should work best if the structures of the stable clusters and of the bulk are very similar. Since free clusters have rather large closed surfaces due to the many surface sections around the outer cluster atoms it seems advantageous to saturate the free valencies at all sites which are not supposed to represent the real crystal. This saturation can be achieved by simulation with real atoms or pseudoatoms. Alternatively, the free cluster can be embedded in an electric field of point charges, which are an approximate account of the rest of the bulk. In the case of infinite systems, the influence of the ulk can be taken into account by point charges rather than by atoms. This procedure can be used for ionic crystals with atoms of alternating charges. An approach, which preserves the transitional invariance of ideal crystals, is the primitive unit cell (PUC) method. This method uses Bloch functions with many wave vectors, k, to account for the transitional periodicity of the unit cell. However, instead of using complex wave functions it is possible to restrict the calculations to k=0 in k space, and enlarge the unit cell instead [21]. It is common to most applications of these approaches that they restrict themselves to a slab consisting of two or several layers for the representation of the bulk, and this usually suffices to generate a good surface [sh.+was. Early studies by Kunz and co-workers [22] and by Clobourn and Mackrodt [23] used clusters that

were terminated by full ionic charges and the choice of the appropriate charges for the point ions has been discussed for an fcc structure like MgO [24]. In the AIMP method [25] the metal oxide clusters are first embedded, then the rest of the crystal is taken to be full ionic charges. In the following two subsections, we will follow a procedure previously reported for metal oxides [26].

1.2.1.1 Bulk simulation

A finite SrO and CaO crystals of 288 point charges were first constructed. The Coulomb potential along the X and Y axes of these crystals are zero by symmetry as in the host crystals. The ±2 charges on he outer shells listed in Table 1, were then modified, using a fitting rocedure, to make the Coulomb potential at the four central sites closely approximates the Madelung potential of the host crystals, and to make the Coulomb potential at the eight points with coordinates (0,±R,±R) and (±R,0, ±R) where R is half the lattice distance, which for SrO is 2.61A°, and CaO is 2.11A° equal to zero as it should be in the host crystals. With these charges, 0.818566 and 1.601818, the Coulomb potential in the region occupied by the central ions is very close to that in the unit cell of the host crystal.

1.2.1.2 Surface simulation

The low coordinated surface sites of SrO and CaO crystals represented in Fig.1 were generated as follow :

1. All charged centers with cartesian coordinates (±X), (±Y) and (Z≤0) were eliminated to generate a flat surface with 176 charged centers occupying the three dimensional space (±X), (±Y) and (Z≤0).

2. All charged centers with cartesian coordinates (±X), (Y<-1) and (Z>0) were eliminated to generate an edge surface with 121 charged centers occupying the three dimensional space (±X), (Y≥ - 1) and (Z ≤0).
3. All charged centers with cartesian coordinates (X>1), (Y<-1) and (Z>0) were eliminated to generate the Br^- corner surface with 81 charged centers occupying the three dimensional space (X≤ 1), (Y≥ - 1) and (Z≤ 0).

The explicitly considered clusters of Fig.2 were then embedded with in the central region of the crystal surface. All the electrons of the embedded clusters were included in the Hamiltonian of the *ab initio* calculations. Other crystal sites entered the Hamiltonian either as full or partial ionic charges as demonstrated in Table 1.

Table 1: Specification of the finite lattices used for Bulk, Flat, Edge, and Corner surfaces of SrO and CaO.R is half the lattice distance, which for SrO is 2.61 Å and CaO is 2.11 Å and r is the distance of the appropriate shell from the center of the lattice.

	Bulk		Flat		Edge		Corner		
r^2/R^2	Coordinates/R (±X), (±Y), (±Z)	Number of centers	Coordinates/R (±X)(±Y)(Z≤0)	Number of centers	Coordinates/R (±X), (Y≥-1) (Z≤0)	Number of centers	Coordinates/R (X≤1), (Y≥-1), (Z≤0)	Number of centers	Charge |q|
2	1 1 0	4	1 1 0	4	1 1 0	4	1 1 0	4	2
6	1 1 2	8	1 1 2	4	1 1 2	4	1 1 2	4	2
10	3 1 0	8	3 1 0	8	3 1 0	6	3 1 0	4	2
14	3 1 2	16	3 1 2	8	3 1 2	6	3 1 2	4	2
18	1 1 4	8	1 1 4	4	1 1 4	4	1 1 4	4	2
18	3 3 0	4	3 3 0	4	3 3 0	2	3 3 0	1	2
22	3 3 2	8	3 3 2	4	3 3 2	2	3 3 2	1	2
26	5 1 0	8	5 1 0	8	5 1 0	6	5 1 0	4	2
26	3 1 4	16	3 1 4	8	3 1 4	6	3 1 4	4	2
30	5 1 2	16	5 1 2	8	5 1 2	6	5 1 2	4	2
34	3 3 4	8	3 3 4	4	3 3 4	2	3 3 4	1	2
34	5 3 0	8	5 3 0	8	5 3 0	4	5 3 0	2	2
38	5 3 2	16	5 3 2	8	5 3 2	4	5 3 2	2	2
38	1 1 6	8	1 1 6	4	1 1 6	4	1 1 6	4	2
42	5 1 4	16	5 1 4	8	5 1 4	6	5 1 4	4	2
46	3 1 6	16	3 1 6	8	3 1 6	6	3 1 6	4	2
50	5 5 0	4	5 5 0	4	5 5 0	2	5 5 0	1	2
50	5 3 4	16	5 3 4	8	5 3 4	4	5 3 4	2	2
50	7 1 0	8	7 1 0	8	7 1 0	6	7 1 0	4	2
54	5 5 2	8	5 5 2	4	5 5 2	2	5 5 2	1	2
54	3 3 6	8	3 3 6	4	3 3 6	2	3 3 6	1	2
58	7 3 0	8	7 3 0	8	7 3 0	4	7 3 0	2	2
66	5 5 4	8	5 5 4	4	5 5 4	2	5 5 4	1	2
54	7 1 2	16	7 1 2	8	7 1 2	6	7 1 2	4	0.818566
62	7 3 2	16	7 3 2	8	7 3 2	4	7 3 2	2	0.818566
66	1 1 8	8	1 1 8	4	1 1 8	4	1 1 8	4	1.601818
82	9 1 0	8	9 1 0	8	9 1 0	6	9 1 0	4	1.601818
86	9 1 2	16	9 1 2	8	9 1 2	6	9 1 2	4	1.601818
		∑=292		∑=176		∑=120		∑=81	

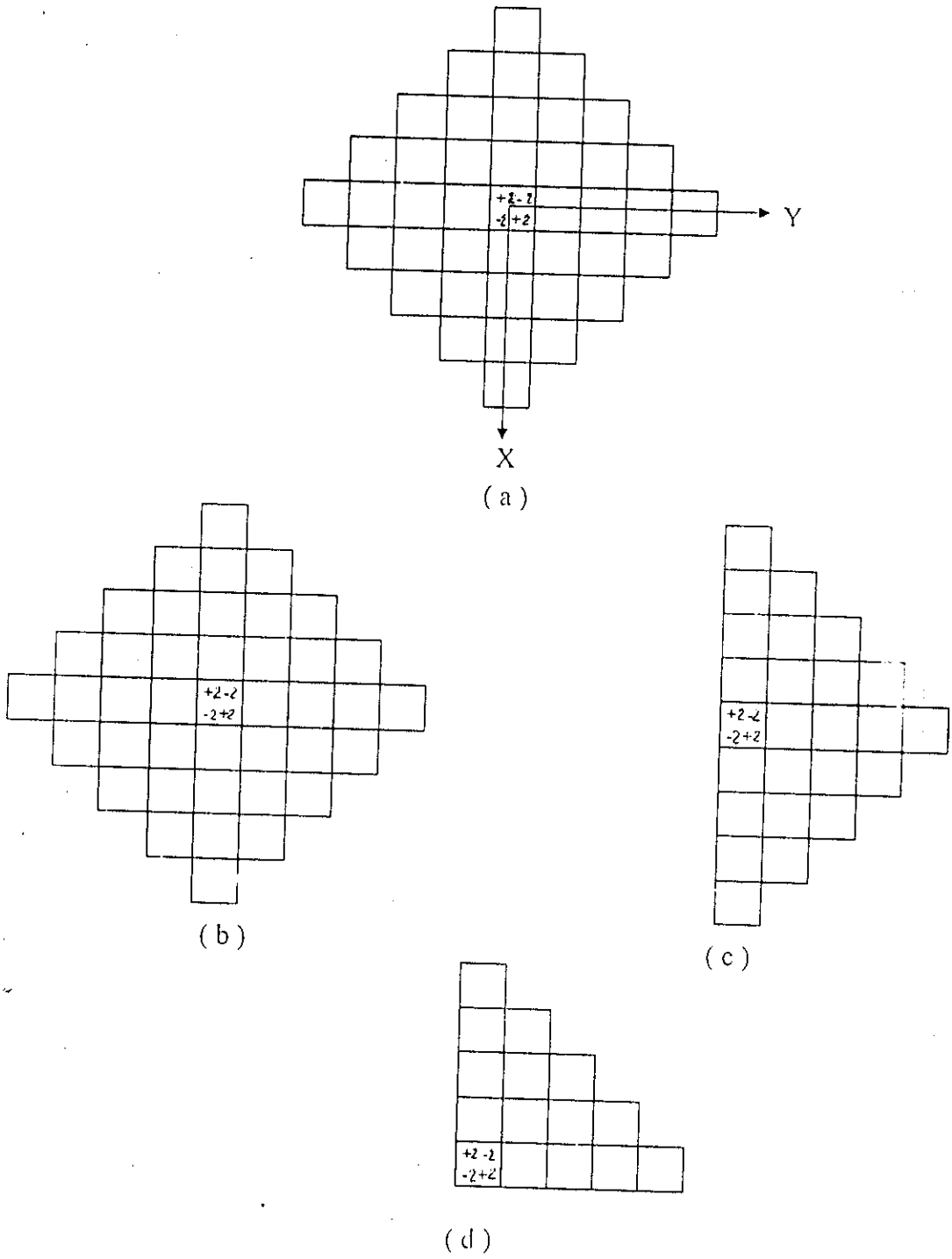

Figure 1: Z = 0 plane representation of the SrO and CaO crystal considered in the calculations.(a) bulk (b) Flat (c) Edge (d) Corner

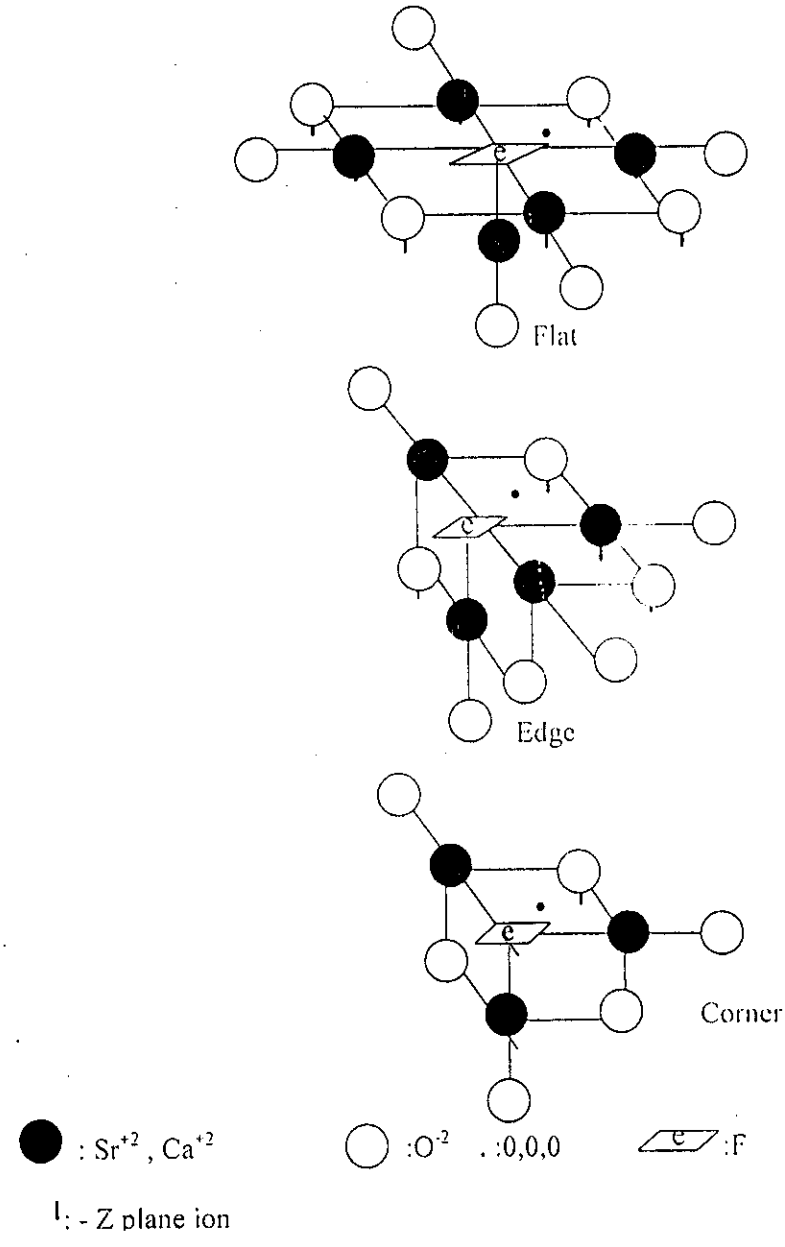

Figure 2: The low coordinated surface clusters considered in the calculations.

1.2.2 Calculations

1.2.2.1 CC diagrams

The geometric relaxation of F^+ center in the ground and excited states of an alkaline earth metal oxide is a key quantity for laser activity due tovibronic coupling. In other words, the possible energy level structure of F^+ center electron is influenced by the shape and depth of the electronic binding potential. This potential is determined mainly by the distance and geometrical arrangement of the nearest surrounding lattice ions, which scillate around their equilibrium positions. The ionic equilibrium is different for different electronic states and the electron-phonon coupling and its effect on the optical transitions can be illustrated with the configuration coordinate CC diagram [27]. In the CC diagram, the electronic energies in the ground and excited states are plotted versus the displacement of usually a single configuration coordinate Q which represents a certain localized mode or normal mode of the lattice coupling to the electron. In other words, Q represents the simultaneous inward-outward displacements of the nearest neighbor cations to the defect site from the lattice interionic separation (Q=0.0) along the axes joining them with the defect site. The other ions were retained in their original positions in the lattice. Starting from the doublet ground state of F_A center an optical excitation produces a transition into the excited states at fixed nuclear coordinates assuming Franck-Condon principle i.e. ertical in the configuration coordinate diagram. Due to the Gaussian shaped probability function for the lowest vibrational state, the transition starts with highest probability from the equilibrium position Q_1. The electronic distribution reached after excitation in the excited state is not in equilibrium with the lattice at Q_1. As a consequence the ions oscillate towards new equilibrium position. The vibrational energy will be

dissipated via anharmonicity into lattice phonons and the electron-lattice system will reach the new equilibrium position Q_2, the relaxed excited state RES. After the mean life time the excited electron returns in a vertical emission process to the ground state, and the subsequent lattice relaxation completes the optical cycle [28].

To construct the CC diagrams, the ion clusters representing the F^+ centers at the flat, edge and corner surfaces of SrO and CaO were first embedded in the three dimensional arrays of point ions described in 2.1.1 The representation of the ion clusters considered in the calculations is given in Fig. 2. The absorption and emission energies were then calculated as the difference between the total energies of the ground and excited states. For this purpose the relevant potential energy curves were calculated, then according to the Franck-Condon principle the absorption energy was calculated as that for a vertical transition from the minimum of the relaxed ground state to the excited state (with fixed atomic coordinates). The luminescence energy was calculated in a similar manner. Stokes-shifts were then calculated as the difference between absorption and emission energies.

$$\Delta E_{absorption} - \Delta E_{emission} \qquad (1)$$

1.2.2.2 CI-Singles method

The CIS method was employed for the calculations of F^+ laser activity, exciton (energy) transfer, relaxed excited state RES orientational destruction and reorientational efficiency. The CIS method, named CI-Singles, uses the configuration interaction approach and model excited states as combinations of single substitutions out of the Hartree-Fock ground state. The CI-Singles theory is an adequate zeroth-order treatment

for many of the excited states of molecules. Treatments of large molecular systems can be afforded by the avoidance of integral storage and transformation, and thus the CI-Singles method has a wide range of applicability. A satisfactory exploration of potential energy surfaces and accurate electronic properties of excited states are possible by the use of an analytic CI-Singles gradients [29]. The method does include some electron correlation in the excited states and can provide reasonable accuracy for excitation energies in comparison with the simplest way to find the lowest relaxed excited state in wide gap insulators, namely, the self consistent field calculations of the triplet state [30].

1.2.2.3 DFT method

The density functional theory DFT method was employed for the calculations of F^+ relaxation and formation energies, the differences between the band gaps and exciton bands (Glasner-Tompkins relation), Mulliken charges and photographic sensitization. The DFT calculations were performed using Becke's three-parameter exchange functional B3 with LYP correlation functional [31]. This hybrid functional includes a mixture of a Hartree-Fock exchange with DFT exchange correlation. Originally the functional B includes the Slater exchange along with corrections involving the gradient of the density [32] and the correlation functional LYP is that of Lee, Yang and Parr, which includes both local and non-local terms [33].

1.2.2.4 CEP basis sets

The Stevens, Basch and Krauss compact effective potential CEP basis sets were employed in the calculations [34]. In these basis sets, the double zeta calculations are referred to as CEP-31G and the triple zeta

calculations are referred to as CEP-121G .However ,there is only one CEP basis set defined beyond the second row elements, and the previous two basis sets are equivalent for these atoms. The CEP-121G basis set was employed in the present calculation. For the s- manifold, a quadruple zeta representation of Gaussian type orbitals was found to be necessary to obtain energies with 0.001-0.003 a.u. of large, even-tempered basis set results .For this size expansion ,little accuracy was lost by restricting the s- and p- basis sets for each atom to have a common set of expansions. For the d- manifold, a three GTO fits yeilds eigenfunctions which are <0.001 a.u. different from large, even-tempered results. These potentials and basis sets have been used to calculate the equilibrium structure and spectroscopic properties of several molecules, and the results compared extremely favorably with corresponding all-electron calculations. All of the computations reported in this paper were carried out using Gaussian 98 system [35].

1.3 Color Center Lasers:

The first observation of laser action with color centers as active material was reported in 1965 by Fritz and Menke [36]. All color center lasers realized so far are based on electronic defects, that is electrons bound to acombination of anion vacancies (intrinsic defects), or electrons bound to acombination of anion vacancies and adjacent impurity ions (extrinsic defects). The simplest electronic defect is the *F* center (from the German word Farbe meaning color) consisting of an electron bound to the net positive charge of an anion vacancy, thus forming localized electronic states with hydrogen-like character in the forbidden energy gap. Although F center is not laser active itself, it serves as an important building block for the formation of all laser active "F aggregate centers". The F center will be used as an example to briefly summarized the basic properties of color center [37] which are common to all laser active centers, i.e. structure of the energy level diagram, natrue of the optical transitions and their broading due to electron-phonon coupling.

In Figure (1.1), only the electronic energies are plotted, referenced to the conduction band, while lattice energies are ignored. The lowest energy levels in the ground state ionic configuration (left side of Figure (1.1)) are positioned fairly deep below the conduction band. The fundamental absorption transition energy 1s→2p is in good agreement with the experimentally observed value (2.7eV or 450 nm).

The close proximity of the RES of the *F* center to the conduction band edge has an important consequence for the formation of other defects. Since the separation is only about 0.1eV, F center electrons can be easily thermally excited from the RES into the conduction band at

200-270K crystal temperature depending on the particular host crystal. The empty anion vacancies lift behind can migrate by thermally-activated diffusion and participate in the formation of more complex F aggregate centers.

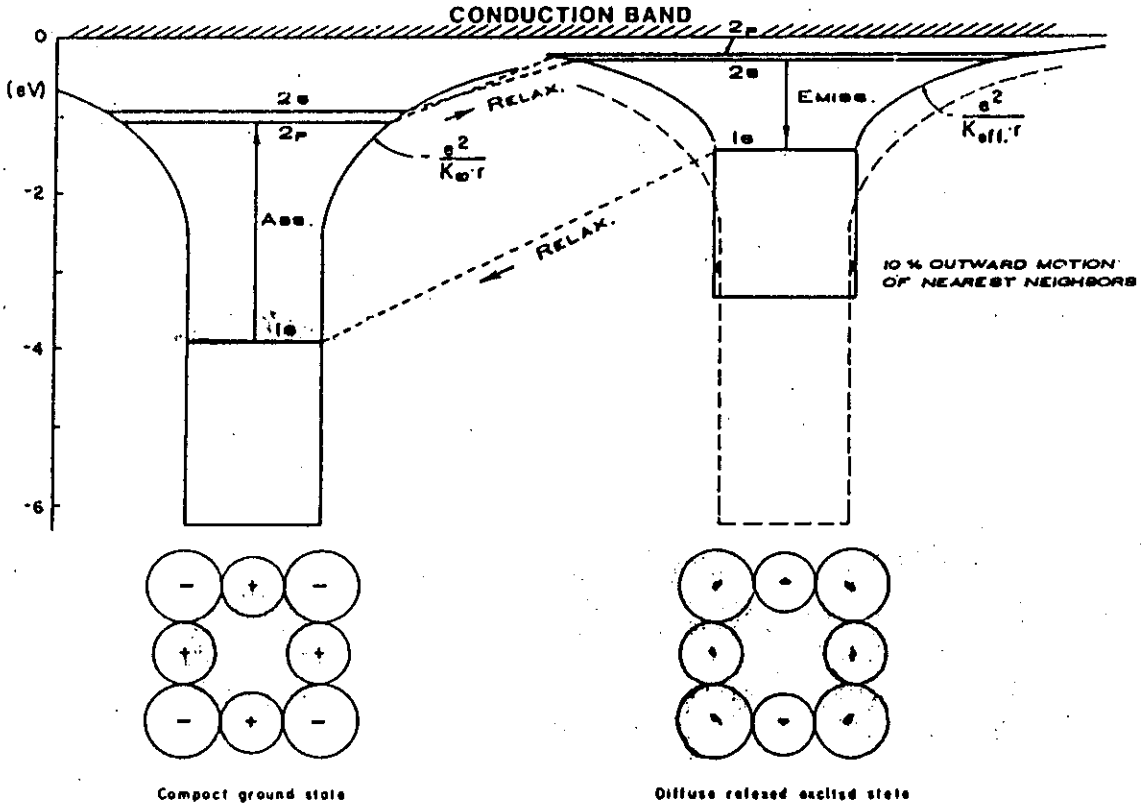

Figure (1.3): Binding potentials and energy levels of the F center electron, shown on the left side for the ground state configuration, and on the right side for the relaxed excited state configuration.

The production of color centers in crystals generally depends on thermal or radiation treatments. One major problem with color centers lasers is the lack of stability of color centers at room tempreture. The mobility of electrons and ions in the host crystals can cause the number of color centers to decay with time or change into aggragate centers.

The possible energy level structure of a color center electron is critically influenced by the instantaneous shape and depth of the electronic binding potential. This potential is determined mainly by the distance and geometrical arrangement of the nearest surrounding lattice ions, which oscillate around their equilibrium positions. On the other hand, the ionic equilibrium positions of the surrounding ions are determined by the average electronic charge distribution. The ionic equilibrium is thus different for different electronic states.

The electron phonon coupling and its effect on the optical transitions can be illustrated with the well known configuration coordinate (CC) diagram [38] illustrated in Figure (1.2) for the case of strong coupling (upper part) and weak coupling (lower part). In the CC diagram the electronic energies in ground and excited state are plotted vs the displacement of usually a single configuration coordinate Q. Within the harmonic approximation the electronic states are parabolas. The strength of the electron phonon coupling is reflected by the different equilibrium positions of the parabolas. For strong coupling the shift is large and for weak coupling it is small.

Starting from the ground state, an optical excitation of the color center produces a transition into the excited state at fixed nuclear coordinates (Franck-Condon principle). Due to the gaussian-shaped probability function for the lowest vibrational state the transition starts with highest probability from the equilibrium position Q_1. The electronic distribution reached after excitation in the excited state is not in equilibrium with the lattice at Q_1. As a consequence the ions oscillate towards new equilibrium positions. The time needed for this relaxation is in the sub-picosecond range [39]. The electron-lattice system will reach

the new equilibrium position Q_2, the RES. After the mean lifetime, the excited electron returns in a vertical emission process back to the ground state, and a subsequent lattice relaxation completes the optical cycle.

For tunable laser applications the electron-phonon coupling provides the following important properties of color centers:

(1) It produces homogeneously (phonon) broadened and Stokes-shifted optical transition bands

(2) Since the relaxation times are in the subpicosecond range and are therefore several orders of magnitude smaller than the RES lifetime, an almost ideal four energy level scheme exists, in which each center excitation leads to a population inversion between the luminescence levels.

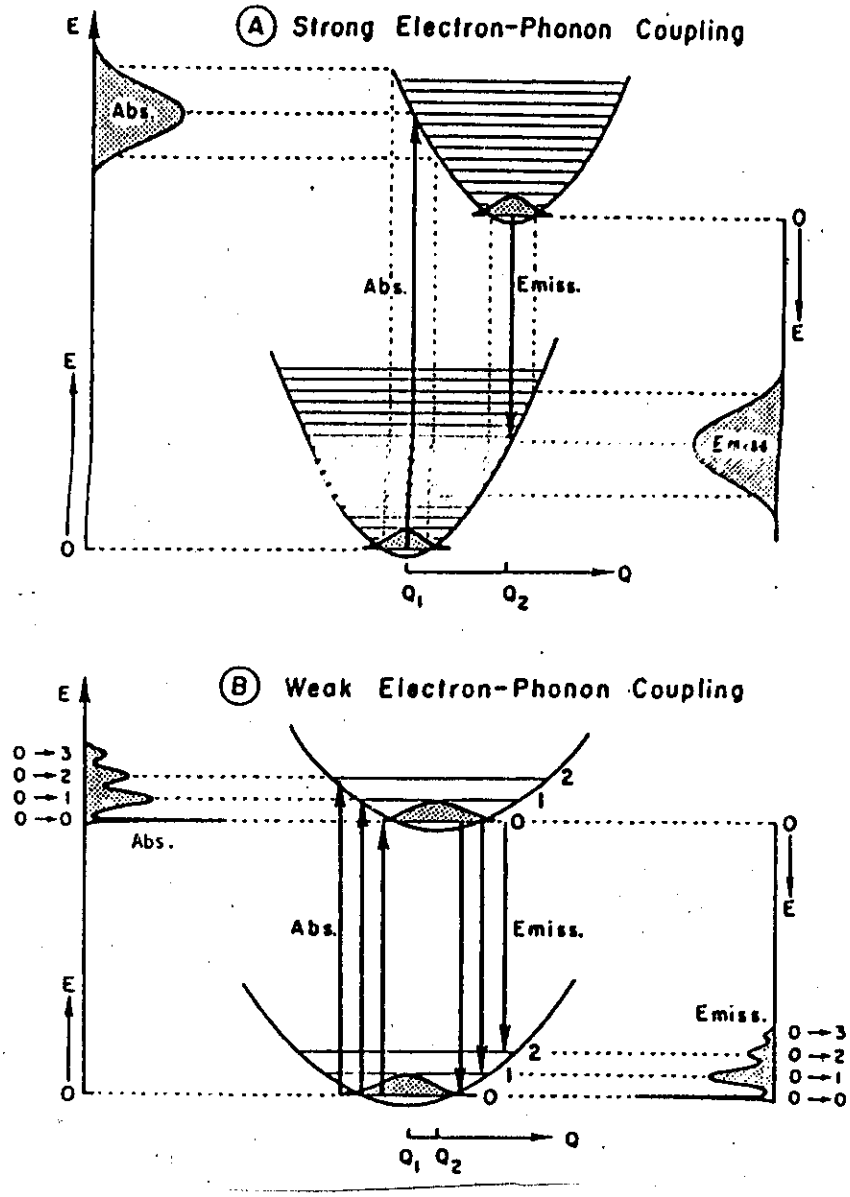

Figure (1.4): Configuration coordinate diagrams for color centers with strong (A) and weak electron-phonon coupling (B), with illustration of band shapes of optical transitions.

1.3.1 The Structure of Color Centers in the Alkali Halides

Alkali halides are ionic crystals having a large forbidden energy gap between valence and conduction bands (~ 8 eV for KCl). Pure crystals are optically transparent over a corresponding wide spectral range limited in the ultraviolet by electronic excitation of the halide ions

and in the infrared by excitation of lattice vibrations. Melting points of the crystals are below 1000°C and thus still in a convenient temperature range for crystal growth. Large single crystals are easily grown from alkali halide powders, with high chemical purity and also high optical quality.

The most important physical property of any material considered for tunable laser applications is the existence of strong and broad optical transitions. Color centers in alkali halides fulfil this requirement particularly well. In general, electrons associated with the defect interact strongly with the surrounding vibrating crystal ions, resulting in optical transitions which are allowed in a broad band around a defect specific central transition wavelength. Duo to the large variety of available defect types and host lattices, optical transitions can be found which cover a wide and important wavelength rang from ~ 0.3 to 4μm.

In the alkali halides, the band gap between the valence and conduction levels is typically 9 to 10 eV. Photons of appropriate energy liberate electrons from the halide ions, simultaneously producing positive holes or simply holes. This process corresponds to an electron being removed from the valence band into the conduction band. Less energetic photons do not ionize the anions but instead excite them into higher excited states. These excitations iinvolve transitions of the valence electrons to exciton states, which produce absorption bands near the fundamental absorption edge of the crystal. The exciton is envisaged as a mobile, uncharged particle consisting of an electron in an excited state bound to a positive hole. As indicated schematically in Figure (1.3), the exciton states lie just below the conduction band.

In order to explain the emission properties of the F center, in particular the anomalously long lifetime (~ 1 μs in NaCl), Fowler assumed that after optical excitation the next-nearest neighboring ions of

the vacancy relax outwards by ~ 10% of their ground state distance (in keeping with the well-known Franck-Condon model). The calculation then results in a strong decrease of the potential well depth and a corresponding shift of the electronic states to higher energies. The total energy of the system (conduction electron plus vacancy) will decrease as the lattice around the vacancy relaxes and phonons are released. So the relaxed excited state (RES) will actually be positioned below the state reached in absorption.

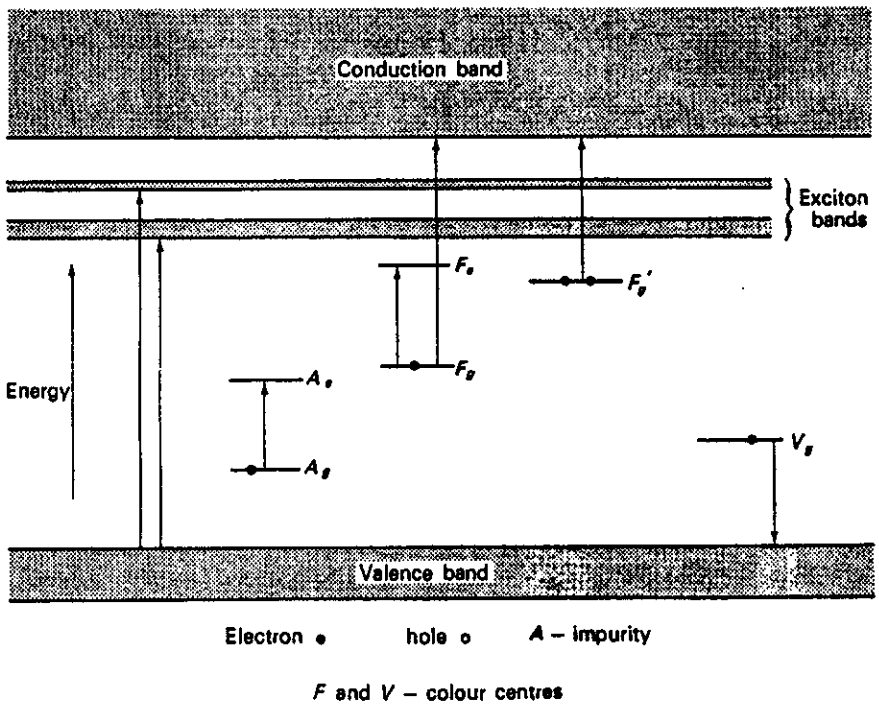

Figure (1.5): Schematic representation of the band structure of an alkali halide crystal, showing transitions associated with the presence of defect levels in the band gap. The subscripts refer to ground (g) and exited (e) states [40].

1.3.1.1 Defect Production Mechanisms

Exposure of alkali halides to ionizing radiation produces in general a large variety of defects. Their individual stability is critically influenced by the purity of the crystal, the temperature, the radiation dose, and the

conditions for thermally induced reactions. In the last few decades a vast amount of background information has accumulated on the detection and identification of most of these radiation induced defects. The most basic problem, to identify and explain the elementary process of defect formation by ionizing radiation at low temperatures in pure crystals, has been investigated in most detail [41, 42].

The presence of impurities can change both the relative concentrations of the defects formed under ionizing radiation and their thermal stabilities. An example is doping with Tl^+ or Ag^+ impurity [43]. Under electron irradiation at low temperatures these ions act as strong electron traps.

Exposure of the radiated crystal to light leads to an excitation of defect electrons. If their final state lies in the conduction band, a transfer of the electron to other defects with electron trapping properties is possible. This causes an ionization of the original defect, which then might become mobile and react with other centers. If the excitation leads to higher bound states, radiationless de-excitations may occur which involve center reorientations and when repeated induce a migration of the center through the lattice.

1.3.2 Laser-Active *F* Aggregate Centers

Figure (1.4) illustrates the ionic structure and electronic charge distribution of the main laser-active defects in their ground and first excited states. All laser-active defects shown here contain the *F* center as the fundamental building block. They can be categorized as:

(1) Type II F_A centers, F_A(II). Here the *F* center is attached to a small Li^+ cationic impurity on a <100> nearest-neighbor site.

(2) Type II F_B centers, F_B(II). In this case the F center is attached to two <100> neighboring Na^+ cations forming a triangular configuration.

(3) F_2^+centers – two anion vacancies sharing one electron.

(4) $(F_2^+)_A$ centers – F_2^+ centers attached to a nearest neighbor Li^+or Na^+ impurity.

(5) (F_2^+)*centers – a defect complex formed from an F_2^+, a divalent cation impurity and a charge – compensating cation vacancy.

(6) F_A(Tl) centers – an F center attached to a <100> neighboring Tl^+ impurity ion having large electron affinity.

In the following section the main optical properties of some of these defects will be described in more detail.

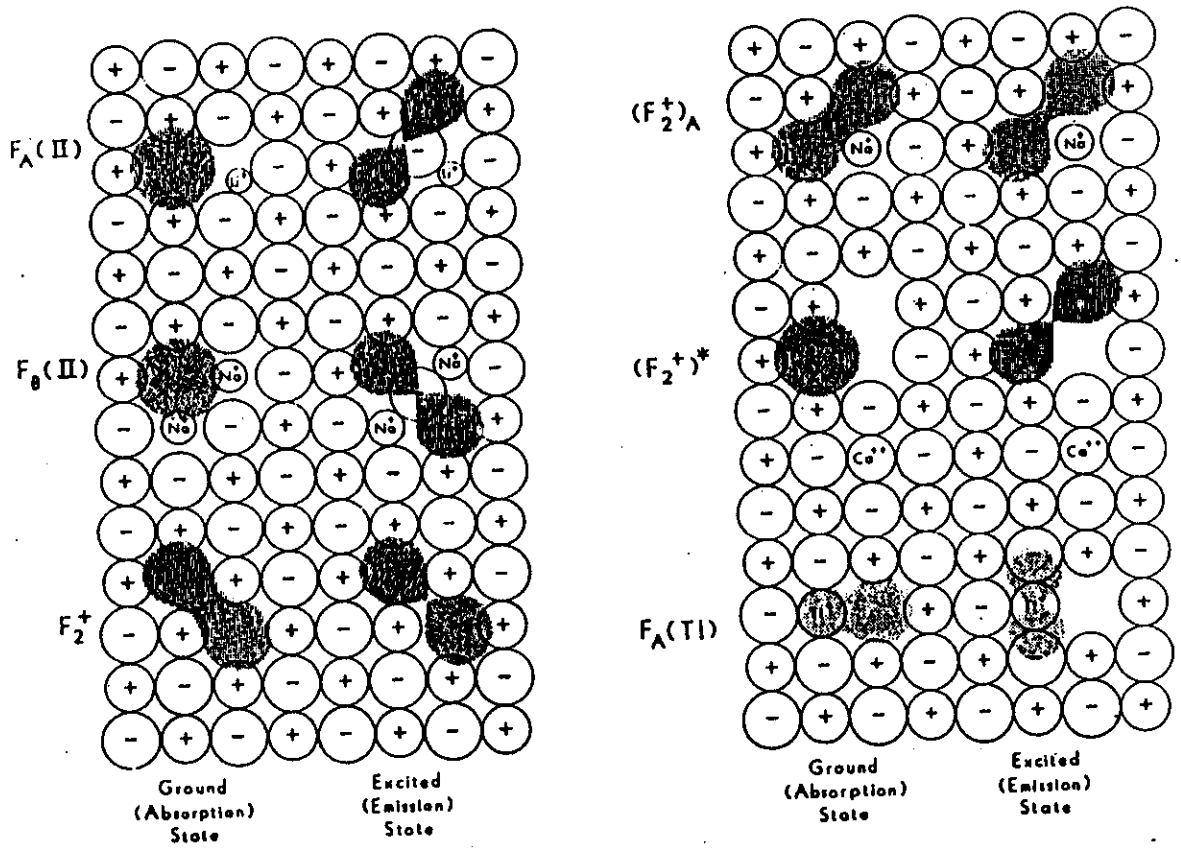

Figure (1.6): Ionic structures of the main laser-active (one electron) F aggregate centers, each shown for ground state and excited state configurations. The shaded areas illustrate the electronic charge distributions.

F_A Centers:

F_A centers can be identified as F centers having an alkali metal impurity as a nearest neighbor and therefore presenting a <100> symmetry axis.

An important example for light-induced center formation processes is the aggregation of F centers into F_A centers in the temperature range of anion vacancy mobility, and effect on the absorption spectrum of a Li^+-doped KCl crystal. Starting from an F center system the incoming photon excites the F center electron and causes its transfer, via the conduction band, to another F center, forming temporarily a vacancy with two electrons (F^- center). The empty anion vacancy is mobile and migrates to the Li^+ impurity where it becomes trapped. This complex will finally re-trap the F^- center electron. As a net result the F center system transforms into an F_A center system, as seen in absorption by disappearance of the F band and formation of the two characteristic F_A band after exposure to light.

In F_A centers [28] the threefold degenerate 2p state of the F center is split in absorption Figure (1.5) due to the adjacent cationic impurity, thus forming two well-resolved absorption transitions (F_{A1} band and F_{A2} band). Two types of centers are distinguished corresponding to the different relaxation behaviour of the centers after optical excitation.

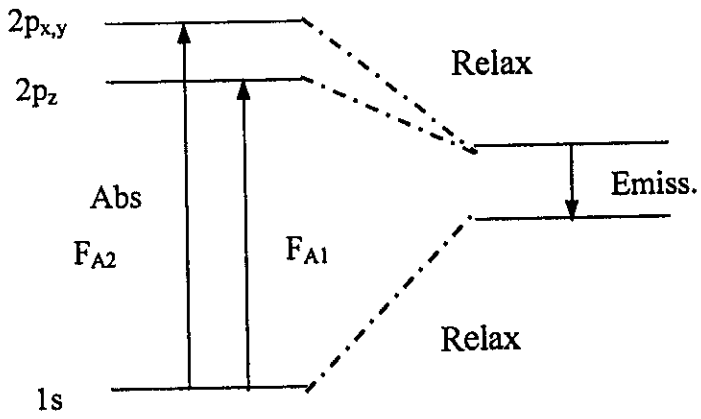

Figure (1.7): Energy level and optical transitions for F_A centers.

In type I F_A centers (F centers attached to large size cationic impurities), the emission band from excitation at either of the two absorption components shows a similar stokes shift to that for the F centers and the life time is also quite similar.

In type II F_A centers (formed if an F center is associated with a small size cationic impurities like Li^+), such as in KCl:Li, the spilitting of the absorption transitions is similar to the type I F_A case but the emission band is very markedly stokes shift and the life time is much shorter than that for the Center.

The behavior of the F_A (II) centers has been attributed to the very strong relaxation of the excited state, which causes a nearest neighbor Cl^- to shift to an interstitial position between two adjacent anion vacancies (saddle–point configuration) in which the electron wave function spreads over the two symmetric wells.

In relation to potential tunable laser applications some effort has been recently devated to the study of F centers attached to monovalent cations other than alkali metals, e.g. Ag^+, Ga^+, Tl^+ and In^+. For Tl^+ -

doped alkali halides, which are some of the most frequently investigated systems [44,45], it has been concluded that Tl^+ F centers complexes with the same structure as F_A centers are formed. However, it appears that for the Tl^+ case the bound electron is about equally shared between Tl^+ ion and the anion vacancy. The electronic structure of these non alkali F_A centers appears to be markedly dependent on the electron affinity of the impurity ion.

F_A (Tl^+) centers:

A previously unknown laser active center was discovered in e^--irradiated crystals containing Tl^+ impurities [46]. The center formed by optical aggregation of an F center to a substitutional Tl^+ impurity, had strong fundamental optical transitions in the near IR between 1 and 2 μm, and was compatible in its polarization behavior with a C_{4v} symmetry defect. Due to its F_A like formation conditions, defect constituents (anion vacancy, (110) neighboring Tl^+ cation and electron) and symmetry properties the defect was termed an F_A (Tl) centers.

The IR wavelength position and small Stokes shift of the fundamental optical transitions indicated that the energy level structure of the F_A (Tl) center had to be quite different from the previously known F_A centers. More specifically, due to the large electron affinity of the Tl^+ impurity, it was proposed that the defect electron had to be at least partially localized at the cationic impurity site [46].

The main optical transitions of the F_A (Tl) centers, identified by the simultaneous growth of the corresponding absorption and emission bands in optical aggregation and thermal annealing steps were measured in seven host lattices [47]. An experimentally determined energy level diagram of the F_A (Tl) center in KCl is shown in Figure (1.6).

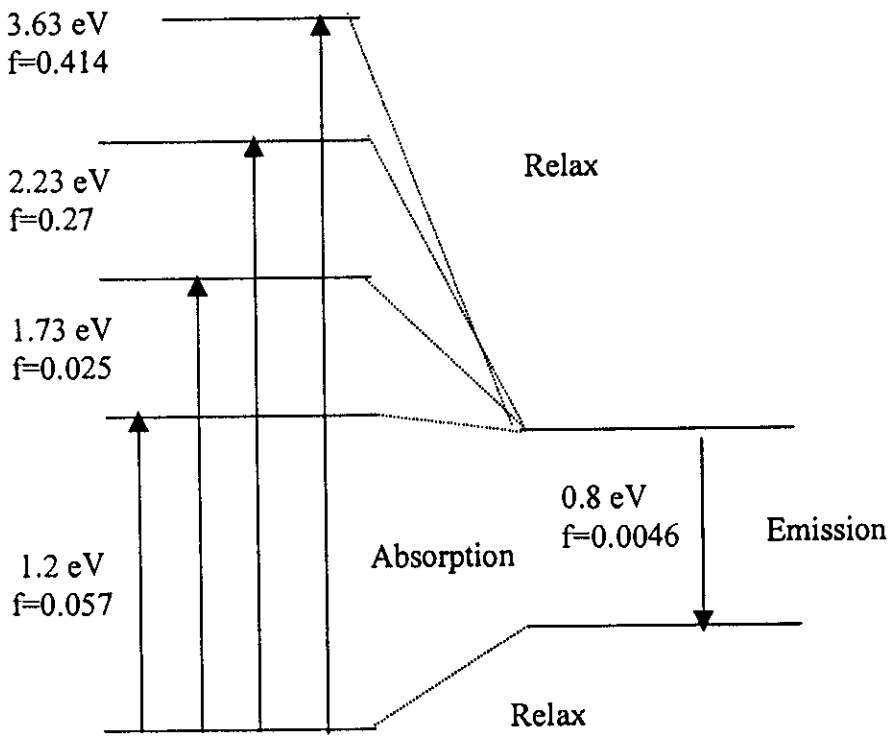

Figure (1.8): Absorption and emission transitions of the F_A (Tl) center in KCl.

After discovery of the F_A (Tl) laser center it was hoped that further stable lasers could be realized with similar F_A centers based on isoelectronic In^+ and Ga^+ impurities and other metal impurities such as Cu^+ and Ag^+. The existence of these defects was known from spin resonance experiments [48, 49].

When replacing a K^+ ion neighbor of a normal F center (in KCl) by the mentioned metal impurity ions (Me^+), the difference in electron affinity Δ of this ion compared with the host ion can be expected to affect the gross features of the electronic structure. For the sequence of ions $Na^+ \longrightarrow Li^+ \longrightarrow In^+ \longrightarrow Tl^+ \longrightarrow Ag^+ \longrightarrow Cu^+$ this difference Δ is rising drastically ($0.8 \longrightarrow 1.1 \longrightarrow 1.4 \longrightarrow 1.7 \longrightarrow 3.2 \longrightarrow 3.4$ eV), and one can expect that with increasing Δ the bound electron will be more and

more removed from the vacancy and bound to the metal ion. For the Na^+ and Li^+ ions (building the classical F_A centers), the electron in its ground state is still mostly centered at the vacancy (and only the excited state is strongly affected by the Δ value).

1.4 Theoretical Models

The approximate solution of the Schrödinger equation is achieved by using two broadly different conceptual approaches. In the first approach, each problem is examined at the highest level of theory currently feasible for a system of its size. In the second approach, a level of theory is first clearly defined after which it is applied uniformly to molecular systems of all sizes up to a maximum determined by available computational resources. Such a theory, if prescribed uniquely of electrons, may be termed a theoretical model, within which all structures, energies, and other physical properties can be examined once the mathematical procedure has been implemented through a computer program.

The model may be tested by systematic comparison of its findings with known experimental results. Depending upon such comparison, a model can acquire some predictive value in situations where experimental data are unavailable.

In the following subsections we will discuss the two theoretical methods employed in the thesis, the density functional theory (DFT) and configuration interaction (CI) CI-singles.

1.4.1 Configuration Interaction CI-Singles.

We begin by selecting the Hartree-Fock single-determinantal wave function, Ψ_{hf}, as a reference for the ground state of the system:

$$\Psi_{HF} = (n!)^{-1/2} \det \{\chi_1\chi_2 \ldots \chi_i\chi_j \ldots \chi_n\} \qquad (1.1)$$

Where n is the number of electrons and χ_p are spin orbitals represented in a convenient basis of N atomic bases functions $\emptyset_\mu$:

$$\chi_p=\sum_{\mu}^{N} C_{\mu p}\,\emptyset_\mu \qquad (1.2)$$

in principle, this reference state need not be the ground state but could be any excited Hf state as well. The following subscript notation will be used throughout: $\mu,\upsilon,\lambda,\sigma,\ldots$, denote atomic bases functions I , j, k, l, …, denote molecular orbitals which are occupied in the ground state; a ,b ,c ,d ,…, denote virtual molecular orbitals, unoccupied in the ground state ; p, q, r, s,…, denote generic molecular spin orbitals. The molecular orbital coefficients ,{ $C_{\mu p}$ },are easily determined by standard self-consistent field (SCF) procedures which solve the Hartree-Fock equations:

$$\sum_{\mu}(F_{\mu\upsilon}-\epsilon_P S_{\mu\upsilon})\,C_{\upsilon p}=0 \qquad (1.3)$$

Here $F_{\mu\upsilon}$ represents the Fock matrix:

$$F_{\mu\upsilon}=H_{\mu\upsilon}+\sum_{\lambda\sigma}\sum_{i} C_{\mu i}\,C_{\upsilon i}(\mu\lambda\|\upsilon\sigma) \qquad (1.4)$$

Given in terms of the one-electron core Hamiltonian, $H_{\mu\upsilon}$ and the usual

$$(\mu\lambda\|\upsilon\sigma)=\iint \emptyset_\mu(1)\,\emptyset_\upsilon(2)(1/r_{12})[\,\emptyset_\lambda(1)\emptyset_\sigma(2)-\emptyset_\sigma(1)\,\emptyset_\lambda(2)]d\tau_1 d\tau_2 \qquad (1.5)$$

$S_{\mu\upsilon}$ represents the overlap matrix:

$$S_{\mu\upsilon}=\int \emptyset_\mu\,\emptyset_\upsilon\,d\tau \qquad (1.6)$$

And ϵ_P is the one-electron energy of orbital p. in these expressions, we have assumed real orbitals throughout. After these equations are solved,

the total energy of the ground-state single determiinant can be expressed as

$$E_{HF}= \sum_{\mu\upsilon}^{HF} P_{\mu\upsilon}^{HF} H_{\mu\upsilon} + 1/2 \sum_{\mu\upsilon\lambda\sigma}^{HF} P_{\lambda\sigma} P_{\mu\upsilon} (\mu\lambda \| \upsilon\sigma) + V_{nuc} \quad (1.7)$$

Where P^{HF} is the HF density given as a sum over the occupied orbitals:

$$P_{\mu\upsilon}^{HF} = \sum_{i=1}^{n} C_{\mu i} C_{\upsilon i} \quad (1.8)$$

And V_{nuc} is the nuclear repulsion energy. Equation 1.1 represents only one of several possible determenants for an electronic wave function of the system. Consider the n(N-n) possible singly excited determinants made by placing an occupied spin orbital with a virtual spin orbital. Such wave functions and associated energies can be written

$$\Psi_{ia} = (n!)^{-1/2} \det \{\chi_1 \chi_2 \cdots \chi_a \chi_j \cdots \chi_n\} \quad (1.9)$$

$$E_{ia} = E_{HF} + \epsilon_a - \epsilon_i - (ia \| ia) \quad (1.10)$$

Where we have introduced the antisymmetrized two-electron integrals in the molecular orbital basis:

$$(pq \| rs) = \sum_{\mu\upsilon\lambda\sigma} C_{\mu p} C_{\upsilon p} C_{\lambda r} C_{\sigma s} (\mu\upsilon \| \lambda\sigma) \quad (1.11)$$

these singly excited wave functions and energies (STA) can be considered first approximations to the molecular excited states of the system. Disadvantages in using (1.9) as a wave function are well-known: (1)it is not an eigenfunction of the spin-squared operator and therefore does not yield pure spin states for closed-shell systems. (2) The spin orbitals involved in the transition have been variationally determined for the ground state. Forcing the virtual orbital to be occupied is more closely

related to ionization rather than excitation. (3) It is not at all appropriate for excitations into degenerate spin orbitals. For instance, the π to π* excited states of benzene can be understood only as a mixture of four singly excited determinants.

$$\Psi_{CIS} = \sum_{ia} a_{ia} \Psi_{ia} \tag{1.12}$$

These configuration interaction (CI) coefficients can be deduced as normalized eigenvectors of the Hamiltonian matrix:

$$< \Psi_{ia} |H| \Psi_{ja} > = [E_{HF} + \epsilon_a - \epsilon_i]\delta_{ij}\delta_{ab} - (ja \| ib) \tag{1.13}$$

we refer to this procedure as full configuration interaction in the space of single substitutions or " CI singles ". eigenvalues, E_{CIS}, of (1.13) are the CI-singles total energies for various excited states. Several points should be made: (1) Ψ_{CIS} is properly orthogonal to the ground-state Ψ_{HF} by virtue of Brillouin's theorem:

$$< \Psi_{ia} |H| \Psi_{HF} > = 0 \tag{1.14}$$

(2)the variational determination of the CI-singles coefficients allows the overall wave function to relax so that Ψ_{CIS} more properly represents an excited state rather than an ionized state; (3) for closed-shell systems, it is possible for Ψ_{CIS} to describe pure sign singlets and triplets (no spin contamination) by allowing positive and negative combinations of α and β excitations from one doubly occupied orbital to one virtual orbital ; (4) CI-singles leads to a well-defined wave function and differentiable energy, thus analytical gradient techniques to determine properties and optimized excited-state geometries are straightforward to apply; (5) CI-singles is also a size-consistent method. This last point is well established, since

it is a property exploited by the various CEPA methods widely used to approximate ground-state correlation energies.

1.4.1.1 Determining the analytical first derivative of the CI-singles Energy

Schemes, which evaluate the gradient of generic CI energies have been available for several years. Indeed, simple modifications of existing programs can be used to generate the gradient of the CI-singles energy. Our emphasis in this section is on the algebraic manipulation of the terms needed for the present case. The simplicity of this special case leads to a technique which will make the computation of excited-state properties for large molecules feasible.

The total energy for a CI-singles excited state is an eigenvalue of the matrix given in (1.13). It can be written as

$$E_{CIS} = E_{HF} + \sum_{ia} a_{ia}^2(\epsilon_a - \epsilon_i) - \sum_{ijab} a_{ja}a_{jb}\,(ja\|ib) \qquad (1.15)$$

The first derivative of E_{CIS} with respect to any external system parameter (for example, a geometric variable or an applied electric field) can be written

$$E_{CIS}^x = E_{HF}^x + \sum_{ijab} a_{ia}^2(\epsilon_a^x - \epsilon_i^x) -$$

$$\Sigma a_{ia}a_{jb}\,(j^{ja^x}a\|ib) + (ja^x\|ib) + (ja\|i^xb) + (ja\|ib^x) \qquad (1.16)$$

Where the superscript x refers to differentiation of the given term with respect to that parameter. The diagonalization of (1.13) ensures that there are not terms involving CI coefficient derivatives. The first term of (1.16) is handled by ordinary HF derivative theory, while the remaining terms

require the knowledge of first-order changes in the Fock and overlap matrices

$$\overset{x}{\epsilon}_p = \overset{x}{F}_{pp} - S_{pp}\,\epsilon_p \tag{1.17}$$

Molecular orbital (MO) coefficient derivatives

$$\overset{x}{C}_{\upsilon p} = \sum_q C_{\upsilon p}\overset{x}{U}_{qp} \tag{1.18}$$

As well as two-electron integral derivatives. The MO coefficient derivatives emerge as bypoducts of solving the coupled-perturbed Hartree-Fock (CPHF) equations for the unknown U matrix

$$\sum_{ia}[1-A_{ijab}]\overset{x}{U}_{ia} = \frac{\overset{x}{Q}_{ih}}{\epsilon_i - \epsilon_h} \tag{1.19}$$

Where Q_{ja} is a perturbation-dependent quantity given in eq 51 of ref 29c and A_{ijab} is a matrix involving transformed two-electron integrals:

$$A_{ijab} = \frac{(ab\|ij)+(aj\|ib)}{\epsilon_i - \epsilon_h} \tag{1.20}$$

The presence of Q_{ia} in (1.19) implies that the linear equations must be solved separately for each variable in the perturbation (one for each geometric degree of freedom in a geometry optimization). Evaluation of the gradient could proceed in this manner, except that it would be extremely inefficient. Our implementation involves several general enhancements that have been suggested by others. First, we follow the realization of that only one perturbation-independent CPHF equation needs to be solved. Second, we seek to derive an equation which does not require the transformation of the atomic orbitals (a task which has been shown to be cumbersome and unnecessary). Our program does act, however, take advantage of the frozen core approximation described

previously. Calculations requesting a gradient to be evaluated must involve CI configurations from all possible single substitutions. This is feature that may be added in the future. The overall prescription is similar to the way in which gradients of correlated wave functions have been presented. Indeed, the final stages of the computational can be handled by the same routines.

We can recast the CI-singles gradient in the following form:

$$E^X = \sum_{\mu\nu\lambda\sigma} \Gamma^{CIS}_{\mu\nu\lambda\sigma} (\mu\upsilon|\lambda\sigma)^X + \sum_{\mu\nu} P^{CIS}_{\mu\nu} H^X_{\mu\nu} + \sum_{\mu\nu} W^{CIS}_{\mu\nu} S^X_{\mu\nu} + V^x_{nuc} \qquad (1.21)$$

The first term in eq (1.21) involves the contraction of the two-particale CI-singles density matrix with two-electron integral derivatives. The second term involves the contraction of the CI-singles density matrix with the one-electron Hamiltonian derivatives. The third term is the contraction of an "energy-weighted " denity matrix with the overlap integral derivatives. The final term is the nuclear repulsion energy derivative. The important construct here is the fact that all multiplications are performed in the ato-mic orbital (AO) basis. This suggests that one possible algorithm would begin by evaluating the Γ^{CIS}, P^{CIS}, and W^{CIS} matrices as preliminary qua-ntities and then producing the gradient by a simple contraction with deri-vative integrals of the atomic orbitals. These derivative integrals could be stored on disk or generated as needed (in the usual sense of a direct calcu-lation). What remains in this discussion, however, is the identification of each these prefactor matrices. We will show later how they can be produ-ced without a transformation of the integrals to the MO basis.

The two-particle CI-singles density matrix, Γ^{CIS}, can be written in terms of the HF ground-state density matrix and the ground-to-excited-state transition density matrix, T^{CIS}.

$$\Gamma^{CIS}_{\mu\nu\lambda\sigma} = 1/2[P^{HF}_{\mu\nu} P^{HF}_{\lambda\sigma} + 2\, T^{CIS}_{\mu\nu} T^{CIS}_{\lambda\sigma} - P^{HF}_{\lambda\sigma} P^{HF}_{\mu\nu} - 2\, T^{CIS}_{\lambda\sigma} T^{CIS}_{\mu\nu}] \quad (1.22)$$

P^{HF} is given in eq 2.8 while T^{CIS} can be expressed

$$T^{CIS}_{\mu\nu} = \sum_{ia} a_{ia} C_{\mu i} C_{\nu a} \quad (1.23)$$

The CI-singles excited-state density matrix, P^{CIS} ,is also constructed as a sum of HF and excited-state terms:

$$P^{CIS}_{\mu\nu} = P^{HF}_{\mu\nu} + P^{\Delta}_{\mu\nu} \quad (1.24)$$

Here have introduced P^{Δ}, the CI-singles Δ density matrix. This can also be called a "difference density matrix", since it represents the changes in electronic distribution upon excitation. It is not however, the same as the transition density matrix defined above identification and evaluation of this Δ density matrix is an important step in calculating accurate excited-state properties using the CI-singles framework. As we shall demonstrate, it is the use of the true CI-singles density matrix required by eq (1.21) and not the simple one-particle density matrix (IPDM) which allows the realistic computation of charge distributions, orbital population, first consider the Δ density matrix which would be added to the HF density matrix in order to generate the IPDM for an excited-state. In the MO basis, it is a symmetric matrix with both occupied-occupied (OO) and virual-virual (VV) contributions:

$$P^{\Delta}_{ij} = -\sum_{ab} a_{ia} a_{jb} \quad (1.25)$$

$$P^{\Delta}_{ab} = +\sum_{ij} a_{ia} a_{jb} \quad (1.26)$$

With the occupied-virual (OV) elements all zero. The true CI-singles density matrix required in eq (1.21) will have exactly the same OO and VV contributions, but the OV terms are not all zero. The appearance of these off-diagonal block elements in the excited-state density matrix can be interpreted as orbital relaxation following the initial gross charge rearran-gement due to excitation. That is say, the CI coefficients will by themselves describe some of the gross features of charge redistribution in the excited state, but the response of the wave function to an external perturbation will account for further refinement in electronic properties. These OV terms can be found by solving a single set of CPHF equations:

$$L_{ai} = \sum_{bj}[(ij\|ab)-(ib\|ja)]\, P^{\Delta}_{bj} + (\epsilon_a - \epsilon_i)\, P^{\Delta}_{ai} \tag{1.27}$$

Where the L vector is the CI-singles lagrangian:

$$L_{ai} = C1_{ai} - C2_{ai} + \sum_{kl} P^{\Delta}_{kl}(al\|ik) + \sum_{bc} P^{\Delta}_{bc}(ab\|ic) \tag{1.28}$$

$$C1_{ai} = -2 \sum_{jab} a_{ia}a_{jb}(cb\|ja) \tag{1.29}$$

$$C2_{bk} = -2 \sum_{jab} a_{ia}a_{jb}(ik\|ja) \tag{1.30}$$

It should be noted that the solution of (1.27) as implemented GASSIAN-90 does not require the transformed two-electron integrals to be stored on disk. The appropriate matrix multiplication can be performed in a"direct" fashion, using stored two-electron integrals or regeneration of them each interaction. The total CI-singles Δ density matrix required in (1.24) can be generated by transforming the entire MO basis Δ density matrix defin-ed by (1.25),(1.26) and (1.27).

$$P^{\Delta}_{\mu\nu} = \sum_{pq} P^{\Delta}_{pq} C_{\mu p} C_{\nu q} \tag{1.31}$$

The final term in the CI-singles gradient requires the energy-weighted density matrix. This is also a sum of HF and excited-state terms

$$W^{CIS}_{\mu\nu} = W^{HF}_{\mu\nu} + W^{\Delta}_{\mu\nu} \tag{1.32}$$

The first term has been presented:

$$W^{HF}_{\mu\nu} = \sum_{i} \epsilon_i C_{\mu i} C_{\nu i} \tag{1.33}$$

While the second term can be shown to have OO,VV, and OV contributions in the MO basis:

$$W^{\Delta}_{ij} = p^{\Delta}_{ij} \epsilon_i - S1_{ij} - \sum_{pq} p^{\Delta}_{pq} (ip \| jq) \tag{1.34a}$$

$$W^{\Delta}_{ab} = p^{\Delta}_{ab} \epsilon_a - S2_{ab} \tag{1.34b}$$

$$W^{\Delta}_{ai} = -C2_{ai} - p^{\Delta}_{ai} \epsilon_i \tag{1.34c}$$

Here the only new quantities are the S matrices:

$$S1_{ij} = \sum_{ab} a_{ia} b_{jb} \tag{1.35a}$$

$$S2_{ab} = \sum_{ij} a_{ia} b_{jb} \tag{1.35b}$$

Which involve the product vector

$$b_{jb} = -\sum_{ia} a_{ia} (ja \| ib) \tag{1.36}$$

transformation of this matrix to the AO basis for use in (1.32) is straightforward :

$$W^{\Delta}_{\mu\upsilon} = \sum_{pq} W^{\Delta}_{pq} C_{\mu p} C_{\upsilon q} \qquad (1.37)$$

1.4.1.2 Correlated treatment for excited states

Having suggested the CI-singles level of theory as an adequate zero-order approximation to many excited states, it would useful to have an additional expression which attempts to access what influence the mixing in of other determinants has on the energy and properties of the excited state. These effects might be included in a manner similar to the ground state correlation correction given by MØller-plesset perturbation theory. Recall that for a HF state, the second-order perturbation correction (MP2) to the energy involves a summation over matrix elements between the zeroth-order state and doubly substituted determinants from that state:

$$\Delta E_{MP2} = -\sum_{S}^{doubles} \frac{< \Psi_{HF} |H| \Psi_S >^2}{E_S - E_{HF}} = -1/4 \, \Sigma \frac{(ij \| ab)^2}{\epsilon_a + \epsilon_b - \epsilon_i - \epsilon_j} \qquad (1.38)$$

This summation runs over single substitutions as well, but according to (1.14) those matrix elements will all be zero. This suggests that if the zeroth-order wave function is a CI-singls eigenvector, a plausible second-order correction will again involve single and double substitutions from the reference state. This implies that it should involve doubles and triples from the ground state. One way in which this interaction might be determined is through the following algebraic expression:

$$\Delta E_{CIS\text{-}MP2} = -1/4 \sum_{ijab} \frac{\langle \Psi_{CIS} |H| \Psi_{ijab} \rangle^2}{\epsilon_a + \epsilon_b - \epsilon_i - \epsilon_j - \Delta_{CIS}} - 1/36 \sum_{ijkabc} \frac{\langle \Psi_{CIS} |H| \Psi_{ijkabc} \rangle^2}{\epsilon_a + \epsilon_b + \epsilon_c - \epsilon_i - \epsilon_j - \epsilon_k - \Delta_{CIS}} \quad (1.39)$$

Here is Δ_{CIS} the CI-singes excitation energy, E_{HF}-E_{CIS}. It is important to note that this expression is not derivable from standard perturbation theory but is simply suggested as one way to access the influence of higher determinants on the CI-singles energy. The numerators of (1.39) are given by a linear transformation of the CI-singles amplitudes:

$$\langle \Psi_{CIS} |H| \Psi_{ijab} \rangle = \sum_{ijab} a_{id} \langle \Psi_{ld} |H| \Psi_{ijab} \rangle = u_{ijab} \quad (1.40)$$

$$\langle \Psi_{CIS} |H| \Psi_{ijkabc} \rangle = \sum_{ijkabc} a_{id} \langle \Psi_{ld} |H| \Psi_{ijkabc} \rangle = u_{ijkabc} \quad (1.41)$$

these u vectors can be thought of as correction amplitudes for doubly and triply substituted determinants. They have been derived previously and are used in other correlated methods:

$$u_{ijab} = \sum_{c} [(ab\|cj)a_{ic} - (ab\|ci)a_{jc}] + \sum_{k} [(ka\|ij)a_{kb} - (kb\|ij)a_{ka}] \quad (1.42)$$

$$u_{ijkabc} = a_{ia}(jk\|bc) + a_{jb}(jk\|ca) + a_{ic}(jk\|ab) + a_{ja}(ki\|bc) + a_{jb}(ki\|ca) + a_{jc}(ki\|ab) + a_{ka}(ij\|bc) + a_{kb}(ij\|ca) + a_{kc}(ij\|ab) \quad (1.43)$$

the quantity in (1.39)can be added to E_{CIS} to define a second-order total energy for an excited state, $E_{CIS\text{-}MP2}$ theory. The size consistency of this energy is easily justified from the fact that elements of the u vectors will be zero unless all of their subscripts correspond to orbitals localized on

the same fragment. The method is, however, nonvariational. A corrected excitation energy can be calculated by tacking the difference in this energy from the ground-state MP2 energy. Some caution should be exercised here, since within a given basis set, there is no guarantee that the perturbation series truncated to second-order is directly comparable between ground and excited states. The energy functional provided by second-order procedure should, however, be valuable in determining accurate potential energy surfaces. Also, there is some interest in knowing what effect the second-order correction has on differences between two excited-state energies. Accurate singlet-triplet splittings for a given symmetry type is one possible application. Limiting the widespread use of CI-singles-MP2 is the fact that the method scales as the sixth power of the number of basis functions.

1.4.1.3 Computational considerations

In this section e summarize some of the algebraic and algorithmic details of the CI-singles calculation with particular emphasis on the feasibility and efficiency of direct methods (those requiring no disk storage of two electron integrals). To diagonalize the singles matrix of (1.13), the most computationally demanding step in the Davidson procedure is the vector multiplication of a trial CI-singles vector with the Hamiltonian, shown in (1.36). This is easily accomplished if the two-electron repulsion integrals from an SCF calculation have been transformed to form the MO integrals on disk. For large molecular systems, it may not be possible to store either set of integrals on disk, so it is desirable to form ulate the matrix multiply in the atomic orbital basis. The problem reduces to finding the square matrix, F, such that the matrix multiply given in (1.36) can be performed as

$$b_{ia} = \sum_{\mu\nu} C_{\mu i} C_{\nu a} F_{\mu\nu} \tag{1.44}$$

indeed, the required AO basis matrices are similar to those first programmed in connection with CI involving nonorthogonal orbitals. Consider the use of the CI-singles transition density matrix in the calculation of the contribution of the two-electron integrals to the F matrix:

$$F_{\mu\nu} = \sum_{\lambda\sigma} T_{CIS}[(\mu\nu\|\lambda\sigma)-(\mu\lambda\|\nu\sigma)] \tag{1.45}$$

Each Davidson iteration will require one (two) of these N2 matrices for each excited state in a spin-restricted (spin-unrestricted) calculation. They can be formed by using previously generated AO integrals or via direct recomputation of the integrals each Davidson cycle. The most efficient means of the performing the AO contraction in either case is by first forming the inegrals as an appropriate combination. Subse-quently, the F and T^{CIS} matrices can be back-transformed to the MO basis:

$$F_{pq} = \sum_{\mu\nu} C_{\mu p} C_{\nu q} F_{\mu\nu} \tag{1.46}$$

$$T_{pq}^{CIS} = \sum_{\mu\nu} C_{\mu p} C_{\nu q} T_{\mu\nu}^{CIS} \tag{1.47}$$

Proving a convenient route to the intermediate arrays needed to evaluate the prefactor matrices for a CI-singlles gradient calculation:

$$C1_{ci} = -2 \sum_{a} T_{ai}^{CIS} F_{ac} \tag{1.48}$$

$$C2_{bk} = -2 \sum_{i} T_{ib}^{CIS} F_{ik} \tag{1.49}$$

$$S1_{ij} = -2 \sum_{a} T_{ai}^{CIS} F_{aj} \tag{1.50}$$

$$S2_{ab} = -2 \sum_{i} T_{jb}^{CIS} F_{ja} \qquad (1.51)$$

These expressions indicate how the energy and gradient of a CI-singles state can be evaluated without the need to store or transform two-electron integrals. A computer program has been written to perform the CI-singles gradient calculation as driven by MO integrals on disk, AO integrals on disk, or no integrals on disk. For a large molecular systems where the storage of AO integrals is not possible, the "direct" calculation would provide the only means to derive the excited-state energies and properties in the CI-singles framework.

There are two other performance issues to mention in this section. First, a great deal of savings is realized when the prefactor matrices of (1.21) are symmetrized before the matrix multiplication. second, the diagonalization procedure is parametrized by the convergence criteria. This is the largest absolute difference between elements of final CI-singles eigenvectors and the corresponding elements of those eigenvectors in the previous cycle. In the calculations described here, we have found that an adequate covergence criteria is 10^{-4} when only excitation energies are desired and 10^{-6} when the gradient or properties depending on the gradient are desired. Tighter convergence criteria will greatly increase the cost of the calculation while providing little or no additional information.

1.4.2 Density Functional Theory (DFT)

Density Functional Theory (DFT) has proved very successful in the past two decades or so in describing the static electronic structure of molecules of considerable size, including such properties as bonding energies, potential surfaces, geometries, vibrational structure and charge distributions. In its original form, however, DFT is essentially confined to ground state properties and the response of this ground state to static external perturbations such as electric fields. More recently the theory has been generalized to include the effects of time dependent perturbations (such as radiation fields) leading to Time Dependent Density Functional Theory (TDDFT) which in form looks very similar to Time Dependent Hartree Fock (TDHF). An extra bonus of TDDFT is that it enables us to calculate excitation energies and oscillator strengths in a consistent way, thus freeing DFT from its ground state limitations. Experience in this area is just building up, but the first results are very encouraging. The method will be extended to the description of periodic systems in one dimension (polymers), two dimensions (surfaces and thin layers) as well as three dimensions (solids). The emphasis is on the linear and non-linear optical properties of these systems as well as their excitation spectra (exciton bands). In the case of surfaces the method also allows the calculation of dispersion interactions between the surface and adsorbate molecules. At a later stage the interaction between the nuclear and electronic degrees of freedom (electron-phonon interaction) has been studied using the same techniques.

In 1964, Hobenberg and kohn [50] proved that the ground state molecular energy, wave function, and all other molecular electronic properties are uniquely determined by the electron probability density ρ

(x,y,z), a function of only three variables. The ground state energy E_o is a functional of ρ and writes $E_o = E_o(\rho)$

If the ground state electron density ρ (x,y,z), has been known, it is possible to calculate all the ground state molecular properties from ρ, first find the wave function Ψ and then find ρ by integration; eq.(1.49)

$\rho(x,y,z)=$

$$n \sum_{all\ m_s} \int \ldots \int \left|\Psi\left(x, y, z, x_2, \ldots . z_n, m_{s1} \ldots, m_{sn}\right)\right|^2 dx_2 \ldots dz_n \qquad (2.1)$$

Kohn and Sham [51] showed that the exact ground state purely electronic energy E_o of an n-electron molecule with ground state electron probability density ρ is given by

$$E_0 = -\frac{1}{2}\sum_{i=1}^{n}\left\langle \Psi_i(1)\left|\nabla_1^2\right|\Psi_i(1)\right\rangle - \sum_{\alpha}\int \frac{Z_\alpha \rho(1)}{r_{1\alpha}} dv_1 + \frac{1}{2}\iint \frac{\rho(1)\rho(2)}{r_{12}} dv_1 dv_2 + E_{xc}[\rho] \qquad (2.2)$$

Where $\Psi_i(1)$, i = 1,2,...,n , is the Kohn and Sham orbitals, and the exchange-correlation energy $E_{xc}(\rho)$ is a functional of ρ. The notations $\Psi_i(1)$ and ρ(1) indicate that Ψi and ρ are taken as functions of the spatial coordinates of electron 1. Kohn and Sham also showed that the exact ground state ρ can be found from the Ψ_i's, according to

$$\rho = \sum_{i=1}^{n} |\Psi_i|^2 \qquad (2.3)$$

The Kohn - Sham orbitals are found by solving the one electron equations

$$\hat{F}_{ks}(1)\Psi_i(1) = \varepsilon_{i,ks}\Psi_i(1) \qquad (2.4)$$

Where the Kohn - Sham operator $\hat{F}_{ks}$ is

$$\hat{F}_{ks} = -\frac{1}{2}\nabla_1^2 - \sum_{\alpha}\frac{Z_\alpha}{r_{1\alpha}} + \sum_{j=1}^{n}\hat{J}_j(1) + V_{xc}(1) \qquad (2.5)$$

Where the Coulomb operator $\hat{J}_j(1)$ is defined by

$$\hat{J}_j(1)f(1) = f(1)\int|\Phi_j(2)|^2\frac{1}{r_{12}}dv_2 \qquad (2.6)$$

Where f is an arbitrary function, $|\Psi_j(2)|^2$; is the electron density, and where the exchange-correlation potential V_{xc} is found as the functional derivative of E_{xc}:

$$V_{xc} = \delta E_{xc}(\rho)/\delta\rho \qquad (2.7)$$

If $E_{xc}(\rho)$ is known, its functional derivative is readily found, and so V_{xc} is known. $\hat{F}_{ks}$ Is like the Hartree-Fock operator, except that the exchange operators $-\sum_{j=1}^{n} \hat{k}_j$ are replaced by V_{xc}, which contain the effects of both exchange (antisymmetry) and electron correlation.

For a closed shell ground state, the electrons are paired in the Kohn - Sham orbitals, with two electrons of opposite spin having the same spatial The Kohn - Sham orbital.

Substitution of eq.(1.53) in (1.52) and use of (1.54) and (1.51) gives

$$\left(-\frac{1}{2}\nabla_1^2 - \sum_{\alpha}\frac{Z_\alpha}{r_{1\alpha}} + \int\frac{\rho(2)}{r_{12}}dv_2 + V_{xc}(1)\right)\Psi_i(1) = \varepsilon_{i,ks}\Psi_i(1) \qquad (2.8)$$

There is only one restriction in using the Kohn – Sham equations to find ρ and E: no one knows that the correct functional $E_{xc}(\rho)$ is for molecules.

Various approximate functions $E_{xc}(\rho)$ have been used in molecular DF calculations. To investigate the accuracy of a particular approximate $E_{xc}(\rho)$, it can be used in DF calculations and compares the calculated molecular properties with their experimental values.

If ρ varies very slowly with position, one can show that $E_{xc}(\rho)$ is given by

$$E_{xc}^{LDA}(\rho) = \int \rho(x,y,z)\varepsilon_{xc}(\rho)dxdydz \qquad (2.9)$$

Where the integral is over all space and $\varepsilon_{xc}(\rho)$ is the exchange plus correlation energy per electron in a homogeneous electron gas with density ρ. A homogeneous electron gas is a hypothetical electrically neutral, infinite volume system consisting of an infinite number of electrons moving in a space throughout which positive charge is continuously and uniformly distributed; the number of electrons per unit volume has a non zero value ρ.

In a molecule, the position charge is not uniformly distributed, but is located only at the nuclei, ρ varies rapidly in a molecule, and eq. (15.57) is only an approximation when applied to molecules, an approximation called the local density approximation (LDA). Molecular LAD calculations show only fair agreement with experimental molecular properties. Much better results are obtained with an improved version of the LAD called the local spin density approximation (LSDA); the LSDA uses different orbitals and different densities ρ^{α} and ρ^{β} for electrons with different spins.

How dose one do a DF calculation with E_{xc}^{LDA} ? Starting with an initial guess for ρ, eq. (1.55) can be used with $E_{xc} = E_{xc}^{LDA}$ to find an initial V_{xc} , which is then used in (1.56) to find an initial set of Kohn - Sham orbitals Ψ_i. The initially found Ψ_i's, and so on. Once the calculation has converged, E_o is found from eq (1.50) using the converged ρ and E_{xc}^{LDA} . The dipole moment can be calculated from ρ using eq (1.58)

$$d = -e\int\int\int \rho(x,y,z) r\, dxdydz + e\sum_{\alpha} Z_{\alpha} r_{\alpha} \qquad (2.10)$$

Where r_α is the vector from the origin to the nucleus of atomic number Z_α and r = xi + yj + zk and similarly for other one electron properties. For large molecules, DF calculations are faster than SCF calculations.

LSDA calculations that solved for the Ψ_i's numerically for 13 homonuclear diatomic molecules found average absolute errors of 0.02 Å in R_e, 0.1 eV in D_e, and 3.3% in vibrational frequencies; the results for bond lengths and vibrational frequencies are good, but the D_e values are not satisfactory in several cases (for example F_2, where D_e is calculated as 3.4 eV versus the true value 1.7 eV).

Another commoly used version of the density functional method is the X_α method (the X stands for exchange). Here, the correlation contribution to E_{xc} is neglected and (based on the homogeneous electron gas model) the exchange contribution is taken as

$$E_{x\alpha} = -\frac{9}{8}\left(\frac{3}{\pi}\right)^{1/3} \alpha \int\int\int \rho^{4/3}(x,y,z)\; dxdydz \qquad (2.11)$$

Where α is an adjustable parameter; values of α from 2/3 to 1 have been used. Functional differentiation of $E_{x\alpha}$ yields the X_α exchange potential as $V_{x\alpha} = -(3\alpha/2)(3\rho/\pi)^{1/3}$. The X_α equations (1.56) with V_{xc} replaced by $V_{x\alpha}$

can be solved by expansion of the Ψ_i's using a basis set, but this requires a lot of computation. A much more efficient procedure is to solve the X_α equations numerically, using the following technique.

One divides space into several regions by imaging a sphere around each atom and a larger sphere around the entire molecule. Within each atomic sphere, and in the region outside of the molecular sphere, the potential energy terms in (1.56) are averaged over the angles θ and φ so as to produce a spherically symmetric potential energy in each of these regions; in the interstitial region between the atomic spheres and within the molecular sphere, the potential energy is assumed constant. Within each atomic sphere, one uses an α value appropriate to that atom; these are taken as the α values needed for an X_α calculation on the isolated atom to produce an energy equal to the Hartree-Fock energy of that atom.

The X_α method was originally developed by Slater for atoms and is sometimes called the Hartree-Fock-Slater method, since it was viewed as providing an approximation to the Hartree-Fock method. However, the X_α method is best viewed as a special case of the density functional method, and not as an approximate Hartree-Fock theory; for example, the orbital energies obtained in the X_α method donot give good approximations to the energies needed to remove an electron from each of the MOs and differ substantially from SCF orbital energies.